Eur. Phys. J. D (2015) 69: 46
DOI: 10.1140/epjd/e2014-50727-8

THE EUROPEAN PHYSICAL JOURNAL D

Regular Article

Measures for the non-Markovianity of a harmonic oscillator coupled to a discrete bath derived from numerically exact references*

Ulf Lorenz[a] and Peter Saalfrank

Universität Potsdam, Institut für Chemie, Karl-Liebknecht-Strasse 24-25, 14476 Potsdam-Golm, Germany

Received 2nd October 2014 / Received in final form 28 November 2014
Published online 17 February 2015 – © EDP Sciences, Società Italiana di Fisica, Springer-Verlag 2015

Abstract. System-bath problems in physics and chemistry are often described by Markovian master equations. However, the Markov approximation, i.e., neglect of bath memory effects is not always justified, and different measures of non-Markovianity have been suggested in the literature to judge the validity of this approximation. Here we calculate several computable measures of non-Markovianity for the non-trivial problem of a harmonic oscillator coupled to a large number of bath oscillators. The Multi Configurational Time Dependent Hartree method is used to provide a numerically converged solution of the system-bath Schrödinger equation, from which the appropriate quantities can be calculated. In particular, we consider measures based on trace-distances and quantum discord for a variety of initial states. These quantities have proven useful in the case of two-level and other small model systems typically encountered in quantum optics, but are less straightforward to interpret for the more complex model systems that are relevant for chemical physics.

1 Introduction

Small systems interacting with a complex environment, a so-called heat bath, are ubiquitous in physics and chemistry. Examples range from quantum optics and information theory [1,2] to the dissipative dynamics of adsorbates at surfaces [3] or excitations in molecular aggregates [4]. The presence of the bath modifies the dynamics of the system in several ways. Two particular effects are decoherence, where the system looses its quantum nature and behaves like a classical statistical ensemble [5], and relaxation, where energy is transferred to the bath degrees of freedom.

A numerically converged ("exact") solution of the time-dependent Schrödinger equation for a system-bath Hamiltonian is only possible for model problems. Therefore, open quantum systems are usually treated by a reduced master equation approach. Here, the system is described by a reduced density operator whose time evolution is governed by a master equation. The interaction with the bath enters through response functions and often takes the form of a time-non-local contribution, i.e., depends on the system density operator at past times. Time-non local master equations are often as hard to solve as the original problem, so a popular, simplifying approach is the Markov approximation, which can be rigorously justified for weak system-bath coupling. Within this approximation memory is ignored, leading to master equations of Redfield or Lindblad forms [4,6], which can be easily solved. While Redfield equations are more straightforward to derive for a specific problem, they can lead to negative populations, which the Lindblad form avoids by construction. The resulting (Lindblad) dynamics largely reduce to rate equations, with coherences and populations of the subsystem decaying on a time scale set by the inverse of the system-bath coupling strength.

However, there is considerable interest in going beyond the Markov approximation. Non-Markovian (NM) quantum channels generally perform more efficiently than their Markovian counterparts [7]. Furthermore, NM baths can lead to uncommon transient thermodynamics regimes [8], and can improve the prospect of controlling quantum systems by optical means [9,10]. In general, it is therefore of considerable practical value to be able to judge on (non-)Markovian behaviour of a given system-bath problem.

Recently, several measures have been proposed to assess the degree of NM dynamics for system-bath situations [11–20]. They are based on certain mathematical properties of the time evolution, notably complete positivity, and therefore refer usually to Markovianity in the context of Lindblad type master equations. In fact, Lindblad master equations are widely used and we will also concentrate on measures related to Lindblad dynamics in

* Supplementary material in the form of one zip file available from the Journal web page at
http://dx.doi.org/10.1140/epjd/e2014-50727-8

[a] e-mail: ulf.lorenz@uni-potsdam.de

what follows. In particular, we shall use trace distances to quantify deviations from Lindblad-type Markovianity. Also, von Neumann entropies as the zero temperature limit of the quantum discord will be considered. Most of these measures originate from quantum information theory, where they have been dominantly applied to single qubits, i.e., two-level systems. Indeed, several measures require expensive calculations that effectively prevent their use for significantly more complex systems.

In this work, we implement several measures for exact system-bath dynamics built on the multi configurational time-dependent Hartree (MCTDH) approach [21], and test them for a non-Markovian, well-converging but nevertheless non-trivial, model system. Specifically, we consider a harmonic oscillator bilineraly coupled to a discretized harmonic bath of 64 environmental oscillators. The MCTDH method, in particular its multi-layer (ML) variant [22] to be used below, is a powerful numerical tool to solve as an exact reference the full system-bath problem [23–27]. The method is general and applicable to complex system-bath Hamiltonians, e.g., with anharmonicities and non-linear couplings [28]. From the exact reference a reduced density matrix can be constructed, and the NM measures can be extracted. Already the coupled harmonic model system, however, serves as a challenging test ground to study how well the previously suggested NM measures perform, in particular when a large variety of initial system states is considered. In fact, it is not a priori clear that computing and interpreting these measures for the situations studied here, is as straightforward as for the (simpler) model systems or initial states studied previously [11–18]. The computability, performance and interpretation of NM measures for complex system-bath Hamiltonians and a large class of initial states, is precisely the focus of this paper.

The paper is organized as follows. The following Section 2 reviews some of the basic mathematical concepts underlying Lindblad master equations, and introduces and discusses several NM measures. In Section 3, we introduce the model system used, and discuss details of the numerical calculations. The results of the calculations are presented in Section 4 and Section 5 summarizes our findings and provides an outlook.

2 Theory

2.1 Lindblad master equations and Markovianity

In this section, we briefly recall some basics of Lindblad master equations and Markovianity to aid in the subsequent discussion (see also Ref. [29]). Consider a system s in contact with some bath b. At some initial time t_0, the state of the system is given in the form of the reduced density operator $\hat{\rho}_s(t_0)$, and we are interested in the state at a later time t. The reduced density operator can be obtained from the total density operator $\hat{\rho}$ by tracing out the bath modes, $\hat{\rho}_s = \mathrm{Tr}_b\hat{\rho}$. The reduced density operator is formally propagated by a dynamical map

$$\Phi_{t,t_0} : \hat{\rho}_s(t_0) \mapsto \hat{\rho}_s(t). \tag{1}$$

To be physical, these maps must be positive and trace-preserving (PT), i.e., they must ensure positive eigenvalues (populations) of $\hat{\rho}_s(t)$ and conservation of the total probability, $\mathrm{Tr}_s\hat{\rho}_s(t) = 1$, respectively. For particular assignments of the system-bath state, they are even completely positive (CP) [19,30].

A compact way of introducing Lindblad master equations starts by assuming that the maps $\Phi_{t,t_0} = \Phi_{t-t_0}$ are linear CPT maps that depend only on the time distance $t - t_0$ [6,31]. Furthermore, for all $t_1, t_2 \geq 0$, they fulfill the semigroup property

$$\Phi_{t_1+t_2} = \Phi_{t_2} \circ \Phi_{t_1} \tag{2}$$

where $\circ$ indicates the subsequent application of Φ_{t_1} and Φ_{t_2}.

The physical meaning is that the time evolution for $t_1 + t_2$ can be broken up into arbitrary steps, where after every intermediate time t_1, the accessible system-bath states are completely characterized by the state of the system only. That is, the bath carries no hidden information about the future of the system, hence it is "memoryless".

Equation (2) can be fulfilled if and only if the system density $\hat{\rho}_s$ evolves according to the Lindblad master equation [29,31]

$$\dot{\hat{\rho}}_s(t) = -i\left[\hat{H}_s, \hat{\rho}_s\right] + \sum_k \gamma_k \left(\hat{V}_k\hat{\rho}_s(t)\hat{V}_k^\dagger - \frac{1}{2}\left[\hat{V}_k^\dagger\hat{V}_k, \hat{\rho}_s(t)\right]_+\right), \tag{3}$$

where atomic units are used here and in the following unless stated otherwise. $\hat{H}_s$ is the system Hamiltonian (including the Lamb-shift from the coupling to the bath), $[\cdot,\cdot]_+$ is the anticommutator, $\hat{V}_k$ are Lindblad operators, and the $\gamma_k \geq 0$ are relaxation or dephasing rates. For example, relaxation from a system state $|n\rangle$ to a state $|n-1\rangle$, can be described by a ladder operator $\hat{V} = |n-1\rangle\langle n|$, and a rate $\gamma_{n\to n-1}$ [27].

We remark that there also exists a form of equation (3) with time-dependent $\hat{H}_s, \gamma_k, \hat{V}_k$. This form comes from a weaker condition of equation (2) that asserts for each $t_0 \leq t_1 \leq t$ the existence of a CPT map Λ_{t,t_1} with the property $\Phi_{t,t_0} = \Lambda_{t,t_1} \circ \Phi_{t_1,t_0}$.

In practice, the derivation of explicit Lindblad equations proceeds via perturbation theory in the system-bath interaction, invoking the Markov approximation, and dropping of oscillating terms (secular approximation). The underlying approximations are $\tau_c \ll \tau_R$ and $\tau_s \ll \tau_R$, where τ_R is a typical relaxation time, τ_s a typical time scale of the system dynamics, and τ_c the so-called coherence or memory time of the bath [4,6]. That is, except for particular cases (e.g., Ref. [32]) the Lindblad form is the exact limit for sufficiently weak coupling and slow system dynamics.

However, real systems with finite system-bath couplings typically show NM dynamics, although this may be a negligible effect. To assess if a Lindblad master equation is valid, one should introduce a NM measure to quantify

how far the actual dynamics stray from Markovian dynamics. With such a measure, we can also study under which modifications the NM dynamics of a system can be enhanced. If the measure allows a time resolution, we may even be able to pinpoint where exactly the NM dynamics occur.

Note, however, that while we can intuitively define NM dynamics *qualitatively* as a violation of equations (2) or (3), there is no unique scheme for a quantitative assignment. To quantify NM dynamics, one monitors a quantity that is known to be zero for a Markovian process, and assigns its value for a particular NM process as NM measure. Examples are information flows from the environment to the system [14,33], or quantities related to the distance to the closest Markovian dynamical map [15] or the accessible state space volume [18]. As a result, there exist several incommensurable NM measures, depending on the monitored property, which may give a different ordering for the NM of a set of dynamical maps. To employ these measures purposefully, it is therefore mandatory that these measures are tested analytically or numerically for exemplary systems.

Finally, we want to point out that an extension to measure non-Markovianity as a violation of Redfield-type master equations is difficult. Such master equations generate non-positive maps, which further complicates the rigorous derivation of NM measures, although existing measures for Lindblad-type NM have been used for Redfield master equations previously [34].

2.2 Trace-distance measures of non-Markovianity

The trace distance between two general states $\hat{\rho}_1, \hat{\rho}_2$ is given by:

$$D\left(\hat{\rho}_1, \hat{\rho}_2\right) = \frac{1}{2}\mathrm{Tr}\left|\hat{\rho}_1 - \hat{\rho}_2\right|, \tag{4}$$

where $|\hat{A}| = \sqrt{\hat{A}\hat{A}^\dagger}$ is the operator with the same eigenvectors as $\hat{A}$, but the absolute value of the corresponding eigenvalues.

CPT maps Φ have the particular property that they do not increase the trace norm between any two states [33],

$$D\left(\Phi\hat{\rho}_1, \Phi\hat{\rho}_2\right) \leq D\left(\hat{\rho}_1, \hat{\rho}_2\right). \tag{5}$$

Since any time evolution in a Markovian system is described by a CPT map, the trace distance between two arbitrary initial system states $\hat{\rho}_{s1}$ and $\hat{\rho}_{s2}$ must be a monotonically decreasing function of time [11]. Any increase in the trace distance is thus a signature of NM dynamics, as suggested by Breuer, Laine and Piilo (BLP) [11,33].

To quantify the degree of non-Markovianity, we choose two initial system states $\hat{\rho}_{s1}, \hat{\rho}_{s2}$, calculate the time derivative of the trace distance, and integrate this derivative over all times where it is positive,

$$M_{\mathrm{BLP}}(\hat{\rho}_{s1}, \hat{\rho}_{s2}) = \int_{t_0}^{\infty} \frac{1}{2}\left[\frac{dD(\hat{\rho}_{s1}(t), \hat{\rho}_{s2}(t))}{dt} + \left|\frac{dD(\hat{\rho}_{s1}(t), \hat{\rho}_{s2}(t))}{dt}\right|\right] dt. \tag{6}$$

For a Markovian system, $dD/dt \leq 0$ for all times and $M_{\mathrm{BLP}}(\hat{\rho}_{s1}, \hat{\rho}_{s2})$ is zero for arbitrary initial system states. In case of NM behaviour, the integrand in equation (6) will have positive segments, leading to $M_{\mathrm{BLP}}(\hat{\rho}_{s1}, \hat{\rho}_{s2}) > 0$. In its original form, the integral is then optimized over all pairs of states to yield a single number for a given system,

$$\mathcal{N} = \max_{\hat{\rho}_{s1}, \hat{\rho}_{s2}} M_{\mathrm{BLP}}\left(\hat{\rho}_{s1}, \hat{\rho}_{s2}\right). \tag{7}$$

We note in passing that similar measures can be set up for every function that is monotonic under the action of a CPT map [12–14,20].

The BLP measure has a rather intuitive interpretation in terms of information flow [33]. A reduction of the trace distance between two states corresponds to a reduced chance of distinguishing them by measurements, hence a flow of information to the environment and vice versa. The value $\mathcal{N}$ is then a quantification of the possible net backflow of information from the environment. As such, it is not only required to be zero for Markovian dynamics, but its absolute value conveys some meaningful information. It should be noted that the condition $\mathcal{N} = 0$ is necessary but not sufficient for the validity of a Lindblad master equation with time-dependent operators [35,36].

A severe problem, however, is the optimization procedure in equation (7). On one hand it is expensive, and while some properties of the optimizing pair are known [37], a naive optimization is still far beyond reach for anything but fewest-level systems. In fact, the question naturally arises what to do in case of a harmonic oscillator, for example, with its infinite number of states. On the other hand, the optimization procedure assigns a single number to the whole state space; if the space can be split into subspaces with very different relaxation behaviour, the BLP measure, equation (7), might not be a very illustrative quantity. Then, time-resolved information such as the quantity $dD(\hat{\rho}_{s1}(t), \hat{\rho}_{s2}(t))/dt$ may be more instructive. Examples of both $M_{\mathrm{BLP}}(\hat{\rho}_{s1}, \hat{\rho}_{s2})$ and $dD(\hat{\rho}_{s1}(t), \hat{\rho}_{s2}(t))/dt$ will be given below.

As an alternative approach, we can start by assuming that the Lindblad master equation contains only time-*independent* operators, i.e., has the semigroup property (2). In this case, we find for an arbitrary initial state $\hat{\rho}_{s0}$ and $\Delta t > 0$

$$\begin{aligned} D\left(\Phi_t\hat{\rho}_{s0}, \Phi_{t+\Delta t}\hat{\rho}_{s0}\right) &= D\left(\Phi_t\hat{\rho}_{s0}, \Phi_t \circ \Phi_{\Delta t}\hat{\rho}_{s0}\right) \\ &\leq D\left(\hat{\rho}_{s0}, \Phi_{\Delta t}\hat{\rho}_{s0}\right). \end{aligned} \tag{8}$$

Equation (8) suggests that instead of using two different initial states, we can then use the same state at two different times t and $t + \Delta t$. This leads to a modified BLP measure,

$$M'_{\mathrm{BLP}}(\hat{\rho}_{s0}, \Delta t) = \int_{t_0}^{\infty} \frac{1}{2}\left[\frac{dD(\hat{\rho}_s(t), \hat{\rho}_s(t+\Delta t))}{dt} + \left|\frac{dD(\hat{\rho}_s(t), \hat{\rho}_s(t+\Delta t))}{dt}\right|\right] dt, \tag{9}$$

where $\rho_s(t) = \Phi_t \rho_{s0}$. In addition, we might do an "inexpensive" optimization over Δt to get

$$\mathcal{N}'(\hat{\rho}_{s0}) = \max_{\Delta t} M'_{\mathrm{BLP}}(\hat{\rho}_{s0}, \Delta t). \tag{10}$$

Formally, this is just a convenient way of replacing the expensive optimization procedure (7) by a simpler one, and assigning a number to each initial state instead of the whole state space. However, it is important to note that the modified measure (10) has a very different interpretation. Non-zero values here indicate that no Lindblad master equation of the form of equation (3) can simulate the exact dynamics for the given initial system state, leaving open the question whether the dynamics are "truly" NM or require time-dependent operators and rates.

2.3 Entanglement-based and related measures of non-Markovianity

Another class of NM measures is based on observing entanglements [16,17]. To quantify the latter, one often adds an additional "blind and dead" [30] so-called ancilla or witness system, and prepares the initial system state such that it is entangled with the ancilla,

$$\hat{\rho}_{sa}(t_0) = |\psi\rangle\langle\psi| \qquad \psi = \frac{1}{\sqrt{N}} \sum_{n=1}^{N} \psi_n^s \psi_n^a, \tag{11}$$

where the ψ_n^s, ψ_n^a are orthonormal states in the system and ancilla space, respectively.

The time evolution is then given by a map $\Phi^s_{t,t_0} \otimes 1_a$, since the ancilla does not participate in the dynamics. If the dynamics are Markovian, Φ^s_{t,t_0} is a CPT map, and the time evolution of the system and ancilla are described by a so-called LOCC operation (local operation with classical communication). It is known that such LOCCs can only decrease the entanglement [38], similar to the trace distance between two states, hence any increase of a suitably chosen entanglement function $E(t)$ over time indicates NM dynamics [17,39,40]. One can then, similar to equation (6), integrate the derivative of the entanglement dE/dt to obtain a single number [17], sometimes called the Rivas-Huelga-Plenio measure M_{RHP} [39].

However, combining this idea with the multi-configuration method used in this work turned out to be rather difficult. Multi-configuration methods are most efficient if there is little correlation between the system and the bath. By preparing the entangled initial state of equation (11), we effectively propagate N initial system states at once, each becoming correlated with the bath in a unique way and requiring an own set of configurations to capture these correlations. This problem can be overcome in principle with a sufficient number of configurations, but test calculations showed that the numerical effort becomes rather large. For more complex systems than a harmonic oscillator, the cost is likely to be prohibitive, therefore we did not investigate this concept any further.

Another measure that seems highly relevant from a theoretical perspective is based on quantum discord. The quantum discord [41] is a non-negative number that measures the amount of information about a "system" (here: the bath) that cannot be extracted by reading out an interacting "apparatus" (here: the subsystem). Lindblad-Markovianity requires zero quantum discord [19], which can be intuitively understood by recalling that the Lindblad formalism assumes that the bath carries no hidden information (i.e., memory). Alipour et al. [16] suggested to use the amount of quantum discord to detect non-Markovianity. They employed a maximally entangled state with an ancilla, and monitored the difference in von Neumann entropies $\Delta_{sa} = S_s - S_a$ as a lower bound of the discord.

However, the specific measure Δ_{sa} suffers from the above-mentioned convergence problem for MCTDH with entangled system-ancilla states. It is also shown in Appendix A that for the factorizing system-bath initial conditions used here, $\Delta_{sa} \leq 0$, and the measure has no predictive power. Furthermore, we show in Appendix B that at zero temperature the quantum discord is simply the entropy of the system ($k_B = 1$ here and in the following),

$$S_s = -\mathrm{Tr}\hat{\rho}_s \ln \hat{\rho}_s. \tag{12}$$

This finding suggests conceptual difficulties with naively applying quantum discord as a NM measure at zero (or possibly low) temperature: even if a Lindblad master equation is used, the reduced system states will always become mixed during the relaxation, giving a non-zero entropy/discord. The question naturally arises, how to derive a useful quantity for non-Markovianity from the entanglement. To study how well suited a quantum discord measure may be, we will also calculate the system entropies and compare them to a rate equation approach.

There are several other measures of NM behaviour that we do not exploit here. Measures that require as input the set of accessible states [18] or the time evolution maps Φ_t [15] are difficult to extend to more than fewest-level state spaces due to the prohibitive cost of computing the input. Further, the so-called quantum Fisher information flow [14] might be an interesting measure. However, its value depends on an inference parameter whose choice is not obvious, therefore we did not include this measure in the present work. Finally, one can introduce measures similar to the BLP or modified BLP measure, but based on the fidelity rather than trace distances [13,20]. We also computed some of these fidelity-based measures for our model problem. While they were quantitatively different from the BLP measure, qualitative conclusions about stability, interpretation etc. were unchanged. Therefore, we also do not further consider these measures from now on.

3 Calculations

3.1 Model system

As a model, we used a harmonic oscillator bilinearly coupled to a bath of N oscillators, with an Ohmic coupling adapted from reference [39] at zero temperature.

The system-bath state is given by a wavefunction of the system coordinate z and the N bath coordinates $\mathbf{q} = (q_1, q_2, \ldots, q_N)$. The wavefunction obeys the time-dependent Schrödinger equation (TDSE),

$$\imath\dot{\psi}(z,\mathbf{q}) = (\hat{H}_\mathrm{s} + \hat{H}_\mathrm{sb} + \hat{H}_\mathrm{b})\psi(z,\mathbf{q}). \tag{13}$$

Here, the system Hamiltonian $\hat{H}_\mathrm{s}$ is a harmonic oscillator,

$$\hat{H}_\mathrm{s} = -\frac{1}{2m_s}\frac{\partial^2}{\partial z^2} + \frac{1}{2}m_s\,\omega_s^2\,z^2 \tag{14}$$

with mass $m_s = 1$ and frequency $\omega_s = 0.4$. The bath was discretized as:

$$\hat{H}_\mathrm{b} = \sum_{b=1}^{N} -\frac{1}{2m_b}\frac{\partial^2}{\partial {q_b}^2} + \frac{1}{2}m_b\,\omega_b^2\,q_b^2 \tag{15}$$

with N equally spaced bath oscillators with masses $m_b = 1$ and $\omega_b = b\Delta\omega = b\frac{\omega_c}{N+1}$. Here ω_c is a cutoff frequency that was set to 1.

The choice of the number of bath modes is based on two considerations. First, replacing a continuous bath by a finite set of oscillators leads to unphysical recurrences [42] with a critical recurrence time $\tau_\mathrm{rec} = 2\pi(N+1)/\omega_c$. This time should be considerably larger than the propagation time, which was chosen as $t_\mathrm{prop} = 70$. Second, to avoid saturation effects, every discretized mode should be typically only excited once. We used $N = 64$ modes with a recurrence time $\tau_\mathrm{rec} \approx 400$. The results did not differ qualitatively if we reduced this to 16 bath modes, suggesting that the calculations are converged with respect to the number of bath modes.

The system is bilinearly coupled to the bath modes,

$$\hat{H}_\mathrm{sb} = \sum_{b=1}^{N} g_b z q_b. \tag{16}$$

In the limit of an infinite number of oscillators, the coupling coefficients g_b are given in the form of a spectral density [23]

$$J(\omega) = \frac{\pi}{2}\sum_{b}^{N}\frac{g_b^2}{m_b\omega_b}\delta(\omega-\omega_b). \tag{17}$$

Here we used $J(\omega) = \kappa\omega\sqrt{1-\omega^2/\omega_c^2}$ from reference [39], which is Ohmic ($J \propto \omega$) up to $\omega \approx 0.5$, and then has a soft cutoff. To stay in the limit of strong coupling, where we can assume the Markov approximation to fail, we chose $\kappa = 0.1$. A "weak-coupling" situation with $\kappa = 0.03$ was also considered. With a finite number of oscillators, we assign the coupling to the continuum of oscillators in the frequency range $[\omega_{b-1}, \omega_b]$ to the bth oscillator. For the equally-spaced oscillators used here, this gives in analogy to [23]

$$g_b^2 \approx \frac{2m_b\omega_b J(\omega_b)}{\pi}\,\Delta\omega. \tag{18}$$

Note that this motivates the use of $N+1$ instead of N in the definition of $\Delta\omega$, otherwise the Nth mode would have frequency $\omega_N = 1$ and a coupling of $g_N = 0$.

A characteristic relaxation rate can be obtained from Fermi's golden rule, which yields after some calculation

$$\gamma = 2\pi\left|\langle f|\hat{H}_{sb}|i\rangle\right|^2\rho(\omega_s) = n\kappa\sqrt{1-\omega_s^2/\omega_c^2} \approx n\kappa. \tag{19}$$

Here, the initial state $|i\rangle$ is given by the nth excited state of the system and a ground state bath, the final state $|f\rangle$ is the $(n-1)$st excited state and a single excitation of a resonant bath mode, and the density of states is $\rho(\omega_s) = 1/\Delta\omega$. Note that in the bilinear coupling model at $T = 0$, all rates except for $n \to n-1$ transitions are zero.

The typical relaxation time (more precisely: state-to-state transition time) is thus $\tau_R \sim 1/\gamma \approx 10/n$ for $\kappa = 0.1$. Already for $n = 1$, this is similar to the typical coherence time $\tau_\mathrm{c} \sim 1/\omega_c = 1$ as well as the typical system time $\tau_s \sim 1/\omega_s = 2.5$, so we would expect noticeable NM contributions to the dynamics. Furthermore, the transition time decreases with increasing quantum number n. Therefore, when higher excited system states $|n\rangle$ are involved, the system-bath coupling becomes effectively larger, and we expect the NM contributions to be even more important. It is certainly interesting to study how well this expectation is reflected in the investigated NM measures.

We want to point out that there are other recent studies on the Markovianity of damped harmonic oscillator models [39,40,43]. In particular, we employed a model Hamiltonian analogous to reference [39]. However, in these references, the solution of the TDSE (13) was performed only for Gaussian states (typically squeezed or thermal states) for which quasi-analytic solutions of the harmonic-bilinear system-bath problem are available. In our work we solve equation (13) fully numerically with the help of the MCTDH method, which offers a larger flexibility in the choice of Hamiltonian and initial states. In particular, we will exploit the flexibility in choosing initial states here.

3.2 Computational details and initial states

For the propagation of the system-bath wavefunction, we used the multilayer version [22] of the multi configurational time-dependent Hartree method [21] (ML-MCTDH) as implemented in the Heidelberg MCTDH package [44,45]. The ML-MCTDH method is based on expanding the total wavefunction into a variationally optimized basis $\phi_{n,s/b}(t)$ for the system and the bath states, so-called configurations or single-particle functions (SPFs), i.e.

$$\psi(z,\mathbf{q},t) = \sum_{i_s=1}^{N_s}\sum_{i_b=1}^{N_b} a_{i_s,i_b}(t)\;\phi_{i_s}^{s}(z,t)\phi_{i_b}^{b}(\mathbf{q},t), \tag{20}$$

where $N_s = N_b$ are the numbers of SPFs for system and bath, respectively. The functions $\phi_{i_{s/b}}^{s/b}$ can then be further expanded in another optimized basis until this scheme terminates in a primitive basis for the system and the individual bath modes. This expansion into optimized orbitals

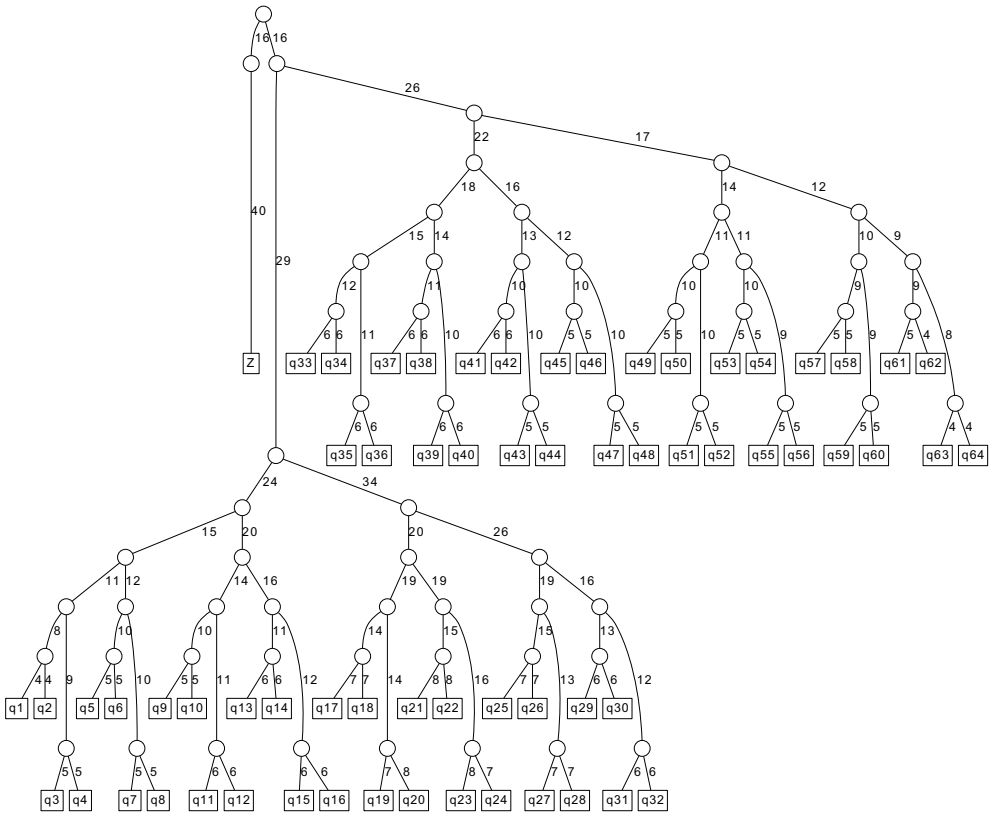

Fig. 1. Example of the multilayer tree for the largest calculation with the e5 initial state in basis 2 (see text). Each circle denotes an expansion into optimized basis functions (SPFs), rectangles denote the respective degree of freedom. The numbers at edges between two circles denote the number of SPFs for the respective (group of) degrees of freedom. Numbers at edges between a circle and a rectangle denote the number of primitive, time-independent basis functions used for that mode. For instance, the system mode (z) is represented by 16 SPFs with 40 primitive (Gauss-Hermite) functions, whereas the 64 bath modes are treated by up to six layers. See reference [22] for further details on the graphs.

can be compactly represented with a tree structure [22], of which an example is shown in Figure 1.

The primitive basis for each degree of freedom consisted of a Gauss-Hermite basis. The choice of the number of primitive basis functions and SPFs will be outlined below. For the propagation, a Bulirsch-Stoer propagator with variational mean field setting was used; deviations from changing the integrator were less than those from changing the number of SPFs. For further details on the numerics, see the Supplementary Material*.

The time derivatives and integration in equations (6) and (9) were done within a linear approximation [46]. That is, with the definition $D_i = D(\hat{\rho}_{s1}(t_i), \hat{\rho}_{s2}(t_i))$, equation (6) becomes

$$M_{\mathrm{BLP}}\left(\hat{\rho}_{s1}, \hat{\rho}_{s2}\right) = \sum_{\substack{i \\ D_{i+1}-D_i>0}} D_{i+1} - D_i, \qquad (21)$$

where the timesteps that were used are $t_i = i\Delta t$ with $\Delta t = 0.05$.

The BLP measure in its original form, equation (7) requires an optimization over the set of initial states $\hat{\rho}_{s1}, \hat{\rho}_{s2}$ of the system, where the optimizing pair is largely unknown. For harmonic oscillators efficient quasi-analytic propagation schemes exist for Gaussian states [17,39,40]. However, since we are considerably more flexible with the ML-MCTDH scheme, we decided to use three sets of initial conditions as a coarse optimization procedure over the state space. In particular, we chose as the initial system states the following:

- excited states of the unperturbed harmonic oscillator, denoted as "ek" for brevity, for the kth excited state;
- displaced states denoted as "dk" generated from displacing the ground state of the unperturbed oscillator by an amount $z_k = 0.6k$;
- squeezed states denoted as "sk" generated from Gaussians centered around the potential minimum and having a width $\Delta z_k = 1.2 + 0.3k$.

For each set of initial conditions, five parameters $k = 1, \ldots, 5$ were used. The parameters for the shifted and squeezed states were chosen such that the initial system state was always dominated by the lowest six states of the unperturbed oscillator. To obtain system-bath initial states to be used in equation (7), for example, the system wavefunction was always coupled to the ground state bath using factorizing initial conditions,

$$\psi(z, \mathbf{q}; t_0) = \psi_s(z) \prod_{b=1}^{N} \psi_{b0}(q_b), \qquad (22)$$

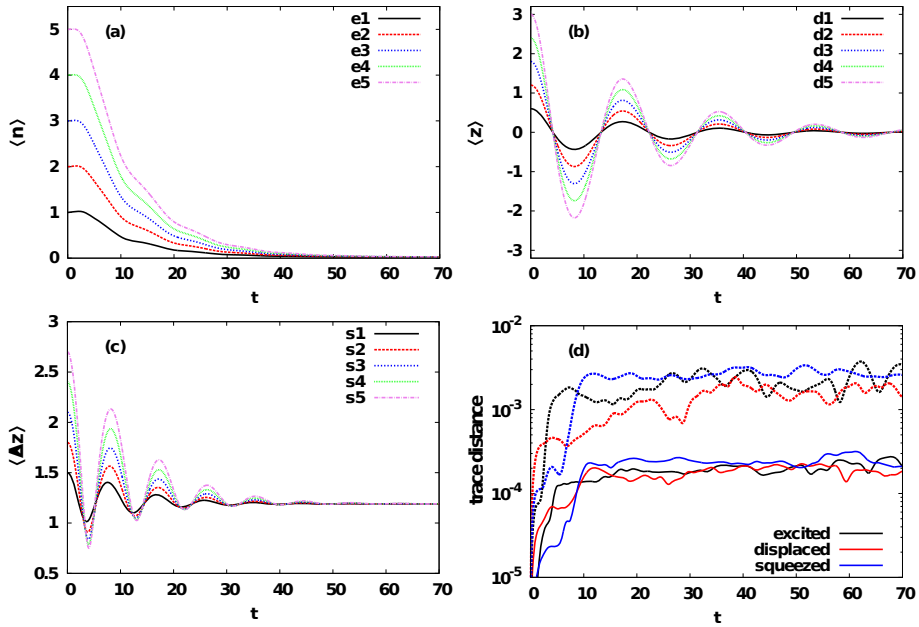

Fig. 2. Dynamics and convergence properties of the system state for the various initial conditions. (a) Average quantum number $\langle n\rangle$ of the unperturbed system oscillator over time for excited state initial conditions. (b) Average position expectation value $\langle z\rangle$ over time for displaced initial conditions. (c) Average position uncertainty $\Delta z = \sqrt{\langle z^2\rangle - \langle z\rangle^2}$ over time for squeezed initial conditions. (d) Convergence of the calculations measured by the trace distance of the system density, $D(\hat{\rho}_{s1}(t), \hat{\rho}_{s2}(t))$, of two calculations with the same initial conditions, but different number of SPFs. For each set of initial conditions, only one curve is shown (e5, d5, s5), the others are qualitatively similar. Solid lines: trace distance between basis 1 and 2. Dashed lines: trace distance between basis 1 and 3.

where $\psi_{b0}(q_b)$ is the ground state of bath oscillator b. Further, propagating the initial system-bath wavefunction (22) under the influence of $\hat{H} = \hat{H}_s + \hat{H}_b + \hat{H}_{sb}$ with ML-MCTDH gives a total wavefunction $\psi(z, \mathbf{q}; t)$, from which the reduced system density can be constructed as $\hat{\rho}_s(t) = \mathrm{Tr}_b|\psi(t)\rangle\langle\psi(t)|$. From the reduced system densities, we determine trace distances according to equation (4) and entropies via equation (12).

We performed three sets of calculations for each parameter k of differing accuracy/size of basis set for the ML-MCTDH scheme.

Basis 1: In a first case, called the "converged calculation" or "basis 1" in what follows, we required for each calculation the smallest natural population η of any node in the multilayer tree to be below 10^{-6}. This was the standard setting.

Basis 2: As a convergence test, we then added 3 SPFs to every single optimized basis. The corresponding ML-MCTDH tree for this basis 2, for the e5 initial system state, is shown in Figure 1.

Basis 3: In a third set, we deliberately relaxed the convergence, and required the smallest natural population to be only below 10^{-4}. This basis can then be used to estimate the stability of the NM measures under numerical errors.

The parameter η determines the number of SPFs. The number of primitive basis functions was identical for all bases. For the system mode z a fixed and well converged number of 40 primitive (Gauss-Hermite) basis functions was used. For the bath modes, the number of primitive basis functions was chosen such that the smallest natural population was always well below 10^{-6}. All three bases were tested for the strong-coupling case with $\kappa = 0.1$.

For weaker system-bath coupling with $\kappa = 0.03$, we employed the same grid and tree parameters as for basis 1 of above, but with a longer total propagation time of $t_{\mathrm{prop}} = 200$ instead of $t_{\mathrm{prop}} = 70$. Since the relaxation time is now increased compared to the memory time of the bath and the system time scale, NM effects should be considerably weaker in this case. These weak-coupling calculations can thus serve as an additional check of how well the magnitude of the measures captures the amount of NM dynamics.

4 Results

4.1 System dynamics

The system dynamics arising from the solution of the TDSE (13) for the 15 different initial conditions (e1-e5, d1-d5, and s1-s5) are shown for various properties in Figures 2a–2c. In all cases, basis 1 has been used as well as $\kappa = 0.1$. In Figure 2a, we show the (sub-)system average eigenstate populations

$$\langle n\rangle = \sum_n P_n\, n \tag{23}$$

where $P_n = \mathrm{Tr}_s(\hat{\rho}_s|n\rangle\langle n|)$ is the population of the nth eigenstate $|n\rangle$ of the unperturbed system Hamiltonian $\hat{H}_s$ ($n = 0, 1, 2, \dots$).

For the excited state initial conditions in Figure 2a, no significant relaxation takes place up to approximately $t = 3$, then the system relaxes on a typical time scale of 10, indicated by the continuously decreasing $\langle n\rangle$ values. In fact, the different curves in Figure 2a are almost identical except for scaling, that is, the relaxation scales with the initial excitation as expected from the golden rule rate, equation (19).

We note that the decay of $\langle n\rangle$ (and consequently, also of the system excitation energy $\omega_s\langle n\rangle$), is not a simple exponential, which has been observed before [27]. This effect is a well-known artefact of factorizing initial conditions [47]. By using factorizing initial conditions, the total system (including the bath) is not in a well-defined thermal state, and over a timescale of the bath correlation time, the subsystem first builds up the discarded correlations with the bath. Effectively, thus the bath state changes considerably for $t < 3$, which is clearly not captured by a Lindblad master equation with time-independent operators and rates.

For the displaced and squeezed initial states (Figs. 2b and 2c), we find a damped motion with relaxation time scales of about 20 and 10, respectively. In particular, Figure 2b shows the system-coordinate expectation value $\langle z\rangle = \mathrm{Tr}_s(\hat{\rho}_s z)$ for the displaced initial system states d1-d5, and Figure 2c the average position uncertainty, $\Delta z = \sqrt{\langle z^2\rangle - \langle z\rangle^2}$ for squeezed initial states s1-s5, where $\langle z^2\rangle = \mathrm{Tr}_s(\hat{\rho}_s z^2)$. In all cases (a)–(c), the system relaxes almost completely to the ground harmonic oscillator state of the system, characterized by $n = 0$, $\langle z\rangle = 0$, and $\Delta z = 1/\sqrt{2m_s\omega_s} = 1.118$.

In Figure 2d we show the convergence of the calculations with increasing basis set size by calculating the trace distance between states represented by different bases. This serves in the end to estimate possible numerical errors of the BLP measures. Specifically, we used the three basis sets 1, 2, and 3 of above, and calculated the trace distances, equation (4) between the system density matrix with basis 1 ($\hat{\rho}_{s1}$) on the one side, and $\hat{\rho}_{s2}$ obtained from either basis 2 (solid lines) or basis 3 (dashed lines), respectively. For clarity, we show results only for e5, d5, and s5 as representative examples; the other calculations gave similar results.

Qualitatively, we note that differences between two bases, measured by their trace distance, build up until around $t = 10$ and then stay constant around some set value. If we compare the "converged calculations" (basis 1) and those with an additional three SPFs (basis 2), the final trace distance is in the range of 10^{-4}–3×10^{-4} [1]. Comparing the calculations with basis 1 and basis 3, we find trace distances of $\sim10^{-3}$. This indicates that in our approach trace distances can be determined with basis 1 with an accuracy in the order of 10^{-4} and slightly above, whereas with at least one order of magnitude smaller accuracy in case of basis 3.

Before discussing the NM measures in the following, we want to briefly summarize properties of the test system that can be used to study these measures:

- The MCTDH calculations converge extremely well, so that the results with basis 1 are essentially numerically exact. From this starting point, we can then deliberately deteriorate the numerical convergence (basis 3) to study how well the NM measures behave under numerical errors.
- There are two distinct ways of modifying the coupling between the subsystem and the bath, which should also affect the degree of NM dynamics. We can change the coupling constant κ to globally modify the system-bath coupling, or we can use higher excited states. This in principle allows a detailed study of the magnitude of the NM measures for different coupling strengths.
- Due to the factorizing initial conditions, there should be significant non-Markovian dynamics for $t < 3$. At least for the e1-e5 states, these should be clearly visible.

4.2 BLP measures of non-Markovianity

We calculated the BLP measure, equation (6), for every pair of initial states. For the 15 initial states, this yields a total of 105 unique pairs. The results are shown in Figure 3, in the form of six blocks e-e, e-d, e-s, d-d, d-s, and s-s, indicating the possible combinations of ρ_{1s} and ρ_{2s} initial states. Each of the three diagonal block consists of $5\times4/2 = 10M_{\mathrm{BLP}}$ values, each of the three off-diagonal block of $5\times5 = 25M_{\mathrm{BLP}}$ values, represented by a colour coding. Although one could maximize (6) over this restricted set of states to obtain an optimized value $\mathcal{N}$ according to (7), it is more instructive to consider the values for the individual pairs. Figure 3a shows the results with basis 1 for the strong coupling case, $\kappa = 0.1$, Figure 3b shows the same for the less accurate basis 3, and Figure 3c for basis 1 again, but with weaker coupling $\kappa = 0.03$.

In all cases shown, the M_{BLP} values are between numerically zero and about 0.008. We note in passing that the values are considerably smaller than those reported in reference [39]. Individual values can vary significantly between basis 1 and 2, especially pairs that involve one excited state. However, in most cases, this affects pairs with small values, so the measure seems to be reasonably stable against variation of the basis set size, i.e., under numerical errors.

If we consider only pairs of displaced states (the d-d block in the center of the figures), the single BLP values are consistently larger for stronger coupling. All of them decrease homogenously by about a factor of three if the coupling is reduced. Further, M_{BLP} increases as the displacement between the two states increases, i.e., if higher excited states are involved. This would suggest that the BLP measure is a monotonic function of the coupling strength between the system and the bath.

[1] We want to point out that this suggests an unusually excellent convergence. When doing similar calculations with a Morse oscillator, we typically reached only convergence with respect to the trace distance of 10^{-3}–10^{-2}.

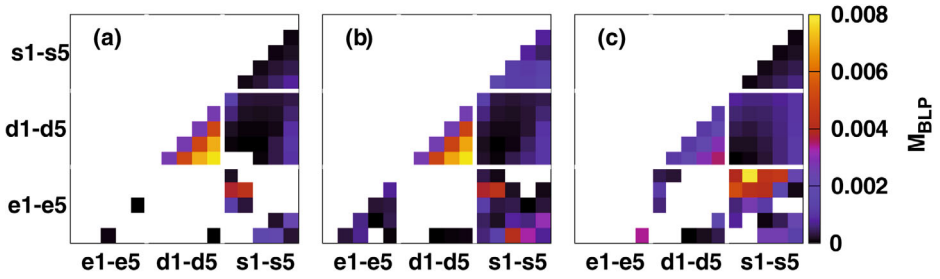

Fig. 3. BLP measure M_{BLP} from equation (6) for all pairs of initial states for (a) "converged" calculations (basis 1), and coupling $\kappa = 0.1$; (b) calculations with relaxed convergence (basis 3), and coupling $\kappa = 0.1$; (c) calculations with basis 1 and weaker coupling $\kappa = 0.03$. Note that the displayed color bar applies only for values $M_{\mathrm{BLP}} > 3 \times 10^{-5}$, otherwise the blocks have been colored white to highlight pairs with negligible values. Only the lower triangle is shown, since the trace distance is invariant under permutation of arguments.

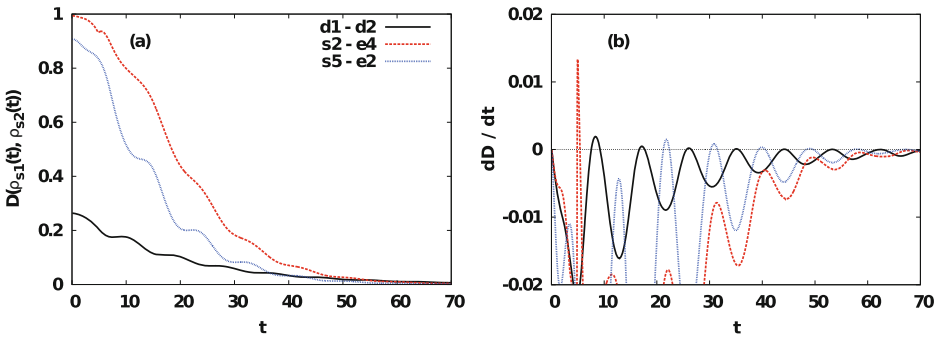

Fig. 4. BLP measure, details of the trace distance for selected pairs of initial states. (a) Trace distance $D(\hat{\rho}_{s1}(t), \hat{\rho}_{s2}(t))$ as a function of time. (b) Time derivatives dD/dt of the initial states in (a).

However, this interpretation fails if we also consider other initial states. Pairs of squeezed states (s-s) or squeezed and displaced states (s-d) give rather small values, which do not show any definite trend. The values involving one excited state initial condition (e-s and e-d) are rather erratic, and pairs of excited state initial conditions (e-e) have usually zero or close to zero measure (indicated by white colour). Also when the system-bath coupling is reduced, the BLP measure for e-s pairs *increases*, which directly contradicts the results from using only displaced states.

Let us study trace distances between different pairs ρ_{s1} and $\hat{\rho}_{s2}$ as well as related quantities in greater (time-resolved) detail. In Figure 4a, we plot the trace distance $D(\rho_{s1}, \hat{\rho}_{s2})$, and in Figure 4b its time-derivative, for the strong-coupling case and three representative state pairs, d1-d2, s2-e4 and s5-e2.

The trace distances start from comparatively large values according to Figure 4a, up to about 1, and then decay towards zero. More important for the BLP measure are the time-derivatives in Figure 4b. They indicate that for two initially displaced states (d1-d2, black curve), the slope of the trace distance increases after every approximately half-period of the oscillation (with the period being $2\pi/\omega_s \approx 16$), with the increases becoming less and less pronounced as the system relaxes. In particular the early maxima of dD/dt dip above the zero-line, i.e., the trace distance increase then and these areas contribute to M_{BLP} indicating non-Markovian behaviour. The resulting M_{BLP} value is 0.0011. One is tempted to correlate the "NM dips" with large $|\langle z \rangle|$ values of the oscillating subsystem, when the system-bath coupling is large.

Several of the calculations showed a different behaviour, similar to the s2-e4 pair (red curve). Here, the trace distance decreases monotonically except for a small spike at $t \approx 5$. The M_{BLP} measure is only 0.00027 in this case.

Finally, we found the pattern, for example for the s5-e2 pair (blue curve), where a periodic increase of the trace distance was observed only for $t \geq 20$, i.e. after approximately twice the relaxation time, when the system is almost settled in the ground state. Nonetheless, for this pair the M_{BLP} value is reasonably large again, 0.0023.

To conclude, we find that for most state pairs, M_{BLP} gives values with no discernible pattern. Also, a study of the time-dependence of the trace distance suggests that similar magnitudes of M_{BLP} can result from very different dynamics. It thus seems unlikely that the optimization procedure of (7) can be circumvented in a reasonable way. That is, conclusions drawn from a restricted set or class of initial states cannot be readily generalized. Considering that we used only few initial states, we will not draw conclusions on the NM dynamics of the system here.

The time-dependence of the trace distance shows oscillatory features that can be readily interpreted as time-dependent signatures of NM dynamics. However, there are also significant exceptions, e.g., the s2-e4 pair in Figure 4a, that are difficult to interpret.

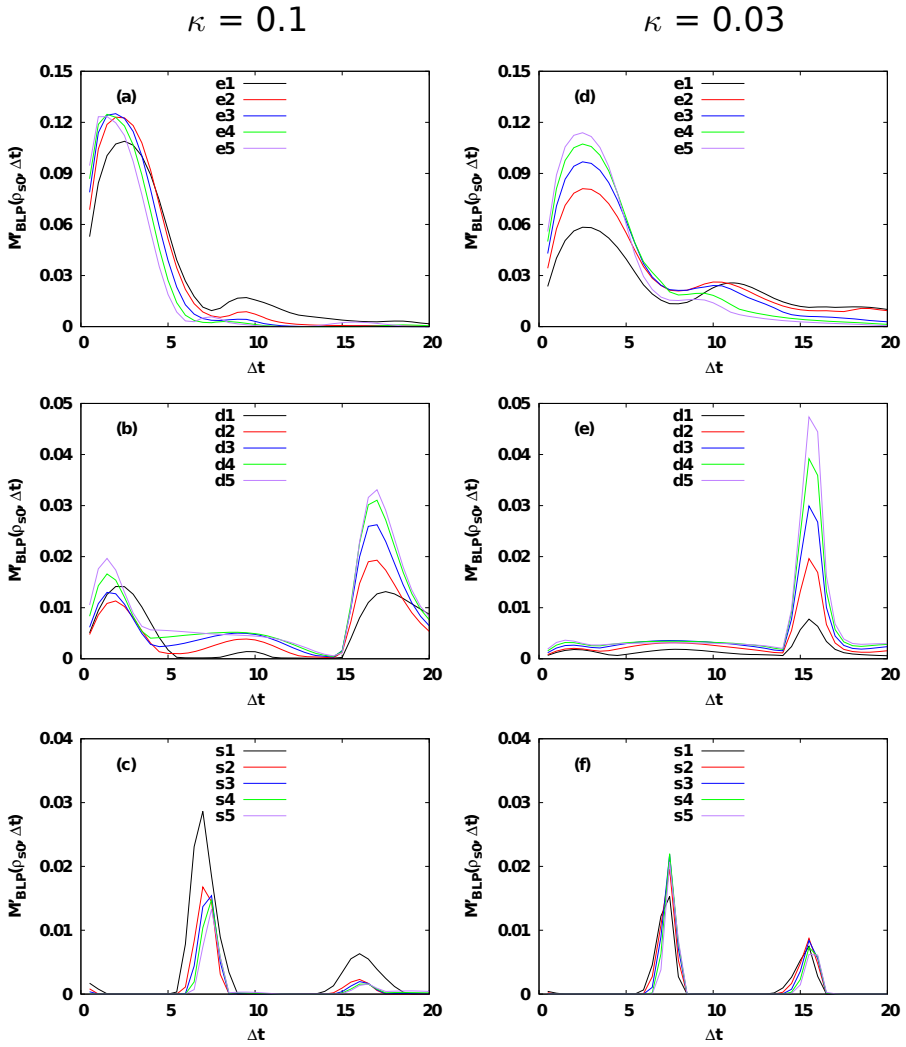

Fig. 5. Modified BLP measure, $M'_{\rm BLP}(\hat{\rho}_{s0}, \Delta t)$, from equation (9) as a function of the time distance Δt for excited initial states ek (a), (d), displaced states dk (b), (e), and squeezed states sk (c), (f), respectively. Note the different scales. (a)–(c) Calculations with strong coupling ($\kappa = 0.1$). (d)–(f) Calculations for weak coupling ($\kappa = 0.03$).

4.3 Modified BLP measure

Figure 5 shows the values for the modified BLP measure, $M'_{\rm BLP}(\hat{\rho}_{s0}, \Delta t)$, obtained from (9) as a function of the time delay Δt for all initial states and for both coupling strengths ($\kappa = 0.1$ and $\kappa = 0.03$). All calculations were done with the converged basis 1, but we remark that the calculations with relaxed convergence (basis 3) gave essentially identical results. Thus, this measure is stable under numerical errors.

We note that the single sets of initial states $\hat{\rho}_s(t_0)$ give considerably different values. Typical values of $M'_{\rm BLP}$ are in the range 10^{-2}–10^{-1}, which is an order of magnitude larger than the values obtained from the original BLP measure, $M_{\rm BLP}$. This probably explains the better numerical robustness of the former.

In all cases there are strong variations of $M'_{\rm BLP}$ with Δt. The excited states ek show the largest values for $\Delta t < 5$. For the displaced states dk, we see two peaks in the range $\Delta t < 5$ and $\Delta t > 15$, and a shallow maximum around $\Delta t = 8$. For the squeezed states sk, there is a dominant peak around $\Delta t = 8$ and a smaller one at $\Delta t = 16$. Note that maxima around 8 and 16 time units correlate with the system's half and full period, respectively. This indicates again, at least for the displaced states, large NM behaviour when the oscillating system couples most strongly with the bath.

Also, we find a tendency of increasing $M'_{\rm BLP}$ values with increasing excitation level of the initial state. However, this correlation is neither linear nor perfect; it is generally more pronounced for weak coupling and for the excited and displaced states. Reducing the coupling strength (Figs. 5d–5f) hardly affects the overall magnitude of $M'_{\rm BLP}$ values, except for the weakly excited initial states e1, d1, s1.

To study the actual dynamics in more detail, we show for $\kappa = 0.1$ the time-dependent trace distance, $D(\hat{\rho}_s(t), \hat{\rho}_s(t+\Delta t))$, and its time derivative, dD/dt in Figures 6a and 6b, respectively. From each set of initial states $\hat{\rho}_s(t_0)$, we picked one calculation (e5, d5, s5) and a value

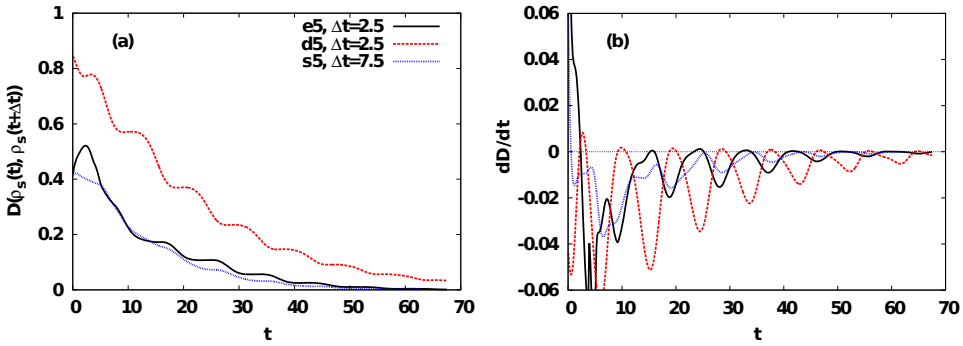

Fig. 6. Modified BLP measure, details of the trace distance for three selected parameters. (a) Trace distance $D(\hat{\rho}_s(t), \hat{\rho}_s(t+\Delta t))$ for selected Δt values, as a function of time. (b) Time derivatives dD/dt corresponding to curves shown in (a).

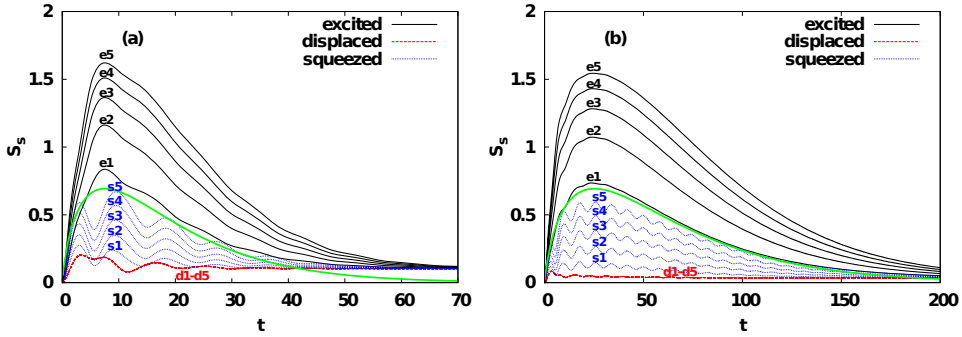

Fig. 7. Von Neumann entropy S_s of the system as a function of time for (a) strong coupling $\kappa = 0.1$ and (b) weak coupling $\kappa = 0.03$. The initial states of the system are excited states (solid black lines), displaced states (dashed red lines) and squeezed states (dotted blue lines). Also shown as solid green curve is the entropy for the e1 state assuming a purely dissipative Markovian bath, equation (24), with the rate from equation (19).

of Δt corresponding roughly to a maximum value in Figure 5. However, we point out that these curves are representative; for other calculations, e.g., e1 instead of e5, the values of the trace distance differed, but the qualitative features were identical.

Similar to the BLP measure in Figure 4, we find an oscillatory behavior of the trace distance, which is most pronounced for displaced states and leads to a periodic increase in the trace distance. We attribute this feature to the fact that the coupling to the bath is strongest at periodic intervals, when the displaced state reaches the classical turning points. An interesting feature appears for squeezed and especially excited initial states, where the trace distance increases initially for $t < 1$ and $t < 5$, respectively. A comparison with Figure 2a suggests that the modified BLP measure is sensitive to the initial non-Markovian buildup of correlations. This feature is absent from the original BLP measure, Figure 4a, which suggests that this process can be captured by a Lindblad master equation with time-dependent operators and rates.

To conclude, the modified BLP measure looks promising. It gives rather large, stable numbers, and due to the dependence on the time shift Δt, we may be able to pinpoint specific time intervals where NM behaviour prevails. The results suggest that the time evolution of the trace distance also gives dynamic information on the NM dynamics.

4.4 Von Neumann entropy

From the ML-MCTDH wave function, we can trivially calculate the system's quantum discord/von Neumann entropy S_s according to equation (12). The results for the 15 initial states considered in this work are shown in Figure 7. We remark that the entropies did not change noticeably with relaxed convergence (using basis 3 instead of 1).

The overall behaviour of S_s as a function of time is similar to that of a similar system-bath Hamiltonian in reference [27]: the entropies start at $S_s(t = 0) = 0$, go through a maximum and then fall off for longer times towards $S_s = 0$ again. This behaviour is due to the fact that we start from a pure state, create a mixed state during the dissipative dynamics, i.e., entanglement with the bath, and end up in a pure state (for zero temperature) for $t \to \infty$ again. By far the largest entropies occur for excited initial states ek, with values ranging from 0.7 to 1.6 (in units of k_B). If we naively interpret the amount of quantum discord/entanglement as a quantitative NM measure, we would conclude from these dynamics that NM dynamics are most pronounced around $t \approx 10$, and less relevant for longer times. Also, the entropy imposes a very intuitive ordering, with larger values for higher excited states and for stronger coupling.

However, the creation of mixed states during dissipative dynamics is not an exclusive feature of NM dynamics. In fact, for a weakly coupled, dissipative, Markovian bath,

reference [27] gives an analytic expression for the entropy of the e1 initial state,

$$S_s = \gamma t\, e^{-\gamma t} - \left(1 - e^{-\gamma t}\right) \ln\left(1 - e^{-\gamma t}\right), \qquad (24)$$

where γ is the relaxation rate, equation (19). The Markovian entropy (24) has a maximum of $\ln 2 = 0.69$ for the maximally mixed state. It is plotted as green curve in Figure 7. We note that the overall shape agrees reasonably well with the exact results, with better agreement for the weaker coupling. From this close agreement, we can conclude that the raw quantum discord/entropy cannot be used as a quantitative NM measure, at least for zero temperature.

For excited initial states, there are two noticable deviations between the Markovian and the exact result. For t between 5 and 20, the exact result gives considerably larger entropies, and for large times, the entropy does not decay to zero, but to a constant value. These effects are present for strong and weak coupling, although considerably smaller in the latter case. For squeezed initial states, the entropy is considerably smaller than for excited initial states. We also find oscillations of the entropy on top of the mean of the curve that appear with a period close to the half-period of the system oscillator. Again, this can be interpreted as a signature of oscillating coupling to, and entanglement with, the bath. For displaced states, only small entropies are observed, and the single curves lie practically on top of each other. Also here, characteristic oscillations emerge.

In conclusion, we find that on first consideration, the entropy/quantum discord as a NM measure has very convenient properties. It is stable under numerical errors, and increases when the coupling constant κ or excitation parameter k is increased. However, Markovian dynamics result in entropies that are very similar to the exact NM case, hence the entropy cannot be used directly as a NM measure. Instead, the deviation between the entropies obtained from Markovian and NM dynamics may possibly be employed as a measure for NM behaviour.

5 Conclusions and outlook

We have calculated the exact short-time dynamics of a damped harmonic oscillator strongly coupled to an Ohmic bath using the ML-MCTDH method. We have further implemented different NM measures for use with the ML-MCTDH method to monitor the degree of non-Markovian dynamics: a trace-distance (BLP) measure, a modified BLP measure, and the quantum discord, which reduces to the system entropy for factorizing initial conditions with zero bath temperature. Some further measures as suggested in the literature, such as ancilla-based entanglement measures, were found to be less suited for this model system or propagation method.

The BLP measure M_{BLP} is straightforward to implement. The values are small for the cases considered here, on the order of numerical errors, but reasonably stable when deliberately reducing the convergence. However, the BLP measure requires an optimization over all pairs of initial states, which in practice can only be carried out over a small subset of states. We found that for most pairs of initial states, there was no discernible pattern concerning the magnitude of the measure, and the result of a maximization could show major variations depending on the chosen set of initial states. This suggests that care should be taken when optimizing the BLP measure only over a subset of initial state pairs, especially if general conclusions are drawn from this subset. The trace distances as functions of time seem to encode some information on the NM dynamics, however, we also find functional dependence that is difficult to interpret.

The modified BLP measure M'_{BLP} offers the prospect of a simpler optimization or of attributing NM dynamics to specific times/time intervals and initial states. Its values are stable under and generally larger than the numerical errors. For several states and time intervals, the results suggest an intuitive interpretation. The underlying trace distance seems to encode details of the NM dynamics, so the measure may be useful to follow NM behavior in time.

The system entropy S_s (quantum discord at zero bath temperature) has several formally useful properties. However, it cannot be directly used to predict the relevance of NM dynamics. In particular for excited initial states, we found considerable entanglement that can also be explained with purely Markovian dynamics. Deviations of the entropy from Markovian behavior may still be useful for interpreting the NM system-bath dynamics, though.

Altogether, all of the measures seem to capture NM dynamics reasonably well, however, they often suffer from problems with interpretation or computation. Considerably more work has to be done to improve our understanding of the quantitative behavior of different NM measures. At present, none of the measures seems to be useable as a black box method that could reliably quantify the NM character of general open quantum systems, i.e., for complex system-bath problems and/or a large variety of initial states.

In further studies, the system-bath coupling should be varied systematically. In particular, more and a larger variety of initial states could be studied, as well as more complex spectral densities. This should shed some light on the quantitative interpretation of the NM measures, which might then be transferable to other open quantum systems.

The authors thank the Deutsche Forschungsgemeinschaft for financial support through project Sa 547/9. UL would like to thank H.D. Meyer for his quick and reliable help with questions related to MCTDH.

Appendix A: Lower bound for quantum discord

The basic idea of the measure suggested in reference [16] is to add an ancilla to the problem whose Hilbert space has the same dimension as the system. The initial state

is then the combined state of the system, the bath and the ancilla. It is set up such that the reduced system-ancilla density matrix is in a maximally entangled state, equation (11) with N being the dimension of the Hilbert spaces. A lower bound for the quantum discord is then obtained by the difference

$$\Delta_{sa}(t) = S_s[\hat{\rho}_s(t)] - S_a[\hat{\rho}_a(t)], \tag{A.1}$$

where $\hat{\rho}_s, \hat{\rho}_a$ are the reduced densities of the system and ancilla, respectively, and S is the von Neumann entropy. If $\Delta_{sa} > 0$, then there is some quantum discord, and the system cannot be described by a Lindblad master equation.

However, it turns out that for the system used here, Δ_{sa} has an exact upper bound of zero. For this, let us start by computing the entropy for the initial ancilla state. Tracing out the system degrees of freedom leaves the ancilla in a maximally mixed state

$$\hat{\rho}_a(t_0) = \mathrm{Tr}_s \hat{\rho}_{sa}(t_0) = \frac{1}{N}\sum_{n=1}^{N} |\psi_n^a\rangle\langle\psi_n^a|, \tag{A.2}$$

with a corresponding value for the entropy of $S_a[\hat{\rho}_a(t_0)] = \ln N$.

If, in addition to equation (11), we assume factorizing initial conditions between the system+ancilla and the bath in the ground state ψ_0^b, then the total wave function is

$$\psi_{\mathrm{tot}}(t_0) = \sum_{i=n}^{N} \psi_n^s \psi_n^a \psi_0^b = \sum_{i=1}^{N} \psi_n^a \psi_n^{sb}. \tag{A.3}$$

Obviously, the states ψ_n^{sb} are orthogonal in the system-bath subspace.

Since the ancilla does not participate in the dynamics by definition, the wave function at some later time can be obtained by simply applying a unitary transformation to the system-bath subspace, and reads

$$\psi_{\mathrm{tot}}(t) = \sum_{n=1}^{N} \psi_n^a \left(\hat{U}(t,t_0)\psi_n^{sb}\right), \tag{A.4}$$

where $\hat{U}(t,t_0)$ is an unitary propagator. Since unitary transformations preserve scalar products, the new set of states, $\hat{U}(t,t_0)\psi_n^{sb}$, forms again an orthonormal basis. The system and bath degrees of freedom can be trivially traced out, and the reduced state $\hat{\rho}_a(t)$ is again a maximally mixed state with a maximum possible entropy of $\ln N$. Consequently, the bound of equation (A.1) can never be larger than zero.

We want to remark that this argument also holds for a bath at finite temperatures, as long as factorizing initial conditions are used. Here we expand the density operator of the bath into its eigenstates ψ_n^e, perform a unitary time evolution (A.3), (A.4), calculate the entropy, and finally statistically average over all result with the Boltzmann weights. Since the entropy of the ancilla is always $\ln N$, the averaging procedure has no effect, and we get the same result as for zero temperature.

Appendix B: Quantum discord at zero temperature

In the following, we want to show that the quantum discord equals the entropy of the system at zero temperature. The quantum discord is defined as [41]:

$$\delta = S_s + S_{sb} + \min_{\{\hat{\Pi}_i\}} \mathcal{S}_{\{\hat{\Pi}_i\}}(\hat{\rho}). \tag{B.1}$$

Here, S_s and S_{sb} denote the entropy of the system and system-bath state, respectively. The last term is the conditional entropy of the bath under an ideal measurement/set of projection operators $\{\hat{\Pi}_i\}$.

To define the conditional entropy, let us consider an orthonormal basis $\{\phi_i^s\}$ in the system space. Then a set of projection operators $\{\hat{\Pi}_i\}$ can be defined as $\hat{\Pi}_i = |\phi_i^s\rangle\langle\phi_i^s| \otimes \hat{1}_b$ with the unit operator $\hat{1}_b$ in the bath space. For each of these operators, we define a conditional bath state under the projection $\hat{\Pi}_i$ as:

$$\hat{\rho}_{b|\hat{\Pi}_i} = \frac{\mathrm{Tr}_s \hat{\Pi}_i \hat{\rho}_{sb}}{p_i} \tag{B.2}$$

with probability

$$p_i = \mathrm{Tr}\hat{\Pi}_i \hat{\rho}_{sb}, \tag{B.3}$$

which can be interpreted as the reduced bath state if the system state has been measured to be $|\phi_i^s\rangle$. The conditional entropy is then given as:

$$\mathcal{S}_{\{\hat{\Pi}_i\}}(\hat{\rho}) = \sum_i p_i \mathcal{S}\left(\hat{\rho}_{b|\hat{\Pi}_i}\right) \tag{B.4}$$

where $\mathcal{S}$ denotes the von Neumann entropy analogous to equation (12).

At zero temperature, the system-bath state is pure for all times and can hence be described by a wavefunction ψ. Therefore the combined system-bath state has zero entropy, $S_{sb} = 0$. It is also always possible to write the wave function in the form of

$$\psi(z,\mathbf{q}) = \sum_i a_i \phi_i^s(z)\phi_i^b(\mathbf{q}), \tag{B.5}$$

where the $\phi_i^{s/b}$ are the (orthonormal) natural orbitals of the reduced system/bath state, i.e., the eigenstates of the reduced density operators, $\hat{\rho}_{s/b} = \sum_i |a_i|^2 |\phi_i^{s/b}\rangle\langle\phi_i^{s/b}|$. To calculate the conditional entropy (B.4), we derive the projection operators from the natural orbitals, $\hat{\Pi}_i = |\phi_i^s\rangle\langle\phi_i^s| \otimes \hat{1}_b$. The conditional bath states are then pure, $\hat{\rho}_{b|\hat{\Pi}_i} = |\phi_i^b\rangle\langle\phi_i^b|$, and the conditional entropy evaluates to

$$\mathcal{S}\left(\hat{\rho}_b|\{\hat{\Pi}_i\}\right) = \sum_i |a_i|^2 \mathcal{S}\left(\hat{\rho}_{b|\hat{\Pi}_i}\right) = \sum_i |a_i|^2 \cdot 0 = 0. \tag{B.6}$$

Plugging these results into equation (B.1) yields the equality of the quantum discord and the entropy, $\delta = S_s$.

References

1. M. Scully, S. Zubairy, *Quantum Optics* (Cambridge University Press, 1997)
2. U. Weiss, *Quantum Dissipative Systems* (World Scientific, 2008)
3. *Dynamics of Gas-Surface Interactions*, Springer Series in Surface Sciences, edited by R. Díez Muiño, H.F. Busnengo (Springer, 2013)
4. V. May, O. Kühn, *Charge and Energy Transfer Dynamics in Molecular Systems*, 1st edn. (Wiley-VCH, 2000)
5. E. Joos et al., *Decoherence and the Appearance of a Classical World in Quantum Theory*, 2nd edn. (Springer, 2003)
6. H.P. Breuer, F. Petruccione, *The Theory of Open Quantum Systems*, 1st edn. (Clarendon Press, 2002)
7. M. Ban, S. Kitajima, F. Shibata, J. Phys. A **38**, 7161 (2005)
8. N. Erez, G. Gordon, M. Nest, G. Kurizki, Nature **452**, 724 (2008)
9. Y. Ohtsuki, J. Chem. Phys. **119**, 661 (2003)
10. D. Sugny, M. Ndong, D. Lauvergnat, Y. Justum, M. Desouter-Lecomte, J. Photochem. Photobiol. A **190**, 359 (2007)
11. H.P. Breuer, E.M. Laine, J. Piilo, Phys. Rev. Lett. **103**, 210401 (2009)
12. A.R. Usha Devi, A.K. Rajagopal, Sudha, Phys. Rev. A **83**, 022109 (2011)
13. A.K. Rajagopal, A.R. Usha Devi, R.W. Rendell, Phys. Rev. A **82**, 042107 (2010)
14. X.M. Lu, X. Wang, C.P. Sun, Phys. Rev. A **82**, 042103 (2010)
15. M.M. Wolf, J. Eisert, T.S. Cubitt, J.I. Cirac, Phys. Rev. Lett. **101**, 150402 (2008)
16. S. Alipour, A. Mani, A.T. Rezakhani, Phys. Rev. A **85**, 052108 (2012)
17. A. Rivas, S.F. Huelga, M.B. Plenio, Phys. Rev. Lett. **105**, 050403 (2010)
18. S. Lorenzo, F. Plastina, M. Paternostro, Phys. Rev. A **88**, 020102 (2013)
19. A. Shabani, D.A. Lidar, Phys. Rev. Lett. **102**, 100402 (2009)
20. R. Vasile, S. Maniscalco, M.G.A. Paris, H.P. Breuer, J. Piilo, Phys. Rev. A **84**, 052118 (2011)
21. H.-D. Meyer, WIREs Comput. Mol. Sci. **2**, 351 (2012)
22. U. Manthe, J. Chem. Phys. **128**, 164116 (2008)
23. M. Nest, H.D. Meyer, J. Chem. Phys. **119**, 24 (2003)
24. R. Martinazzo, M. Nest, P. Saalfrank, F. Tantardini, J. Chem. Phys. **125**, 194102 (2006)
25. H. Wang, M. Thoss, New J. Phys. **10**, 115005 (2008)
26. H. Wang, M. Thoss, Chem. Phys. **370**, 78 (2010)
27. F. Bouakline, F. Lüder, R. Martinazzo, P. Saalfrank, J. Phys. Chem. A **116**, 11118 (2012)
28. I. Andrianov, P. Saalfrank, Chem. Phys. Lett. **433**, 91 (2006)
29. D. Chruściński, Open Syst. Inform. Dyn. **21**, 1440004 (2014)
30. P. Pechukas, Phys. Rev. Lett. **73**, 1060 (1994)
31. G. Lindblad, Commun. Math. Phys. **48**, 119 (1976)
32. F. Giraldi, F. Petruccione, Phys. Rev. A **88**, 042102 (2013)
33. H.P. Breuer, J. Phys. B **45**, 154001 (2012)
34. G. Clos, H.P. Breuer, Phys. Rev. A **86**, 012115 (2012)
35. M. Jiang, S. Luo, Phys. Rev. A **88**, 034101 (2013)
36. D. Chruscinski, F.A. Wudarski, Phys. Lett. A **377**, 1425 (2013)
37. S. Wißmann, A. Karlsson, E.M. Laine, J. Piilo, H.P. Breuer, Phys. Rev. A **86**, 062108 (2012)
38. M.B. Plenio, S. Virmani, Quantum Inf. Comput. **7**, 1 (2007)
39. R. Vasile, F. Galve, R. Zambrini, Phys. Rev. A **89**, 022109 (2014)
40. V. Venkataraman, A.D.K. Plato, T. Tufarelli, M.S. Kim, J. Phys. B **47**, 015501 (2014)
41. H. Ollivier, W.H. Zurek, Phys. Rev. Lett. **88**, 017901 (2001)
42. R. Baer, R. Kosloff, J. Chem. Phys. **106**, 8862 (1997)
43. A. Rivas, A.D.K. Plato, S.F. Huelga, M.B. Plenio, New J. Phys. **12**, 113032 (2010)
44. O. Vendrell, H.D. Meyer, J. Chem. Phys. **134**, 044135 (2011)
45. O. Vendrell, H.D. Meyer, The MCTDH Package, Version 8.5 (2011)
46. U. Lorenz, MCTDH Tools for the Heidelberg MCTDH package (2013), http://sf.net/p/mctdhtools
47. C. Meier, D.J. Tannor, J. Chem. Phys. **111**, 3365 (1999)